analytical chemistry

Article

Cite This: Anal. Chem. 2018, 90, 11131−11137

pubs.acs.org/ac

Identification of Intracellular and Extracellular Metabolites in Cancer Cells Using ^{13}C Hyperpolarized Ultrafast Laplace NMR

Guannan Zhang,[†,∥] Susanna Ahola,[‡] Mathilde H. Lerche,[§] Ville-Veikko Telkki,*[,‡] and Christian Hilty*[,†]

[†]Department of Chemistry, Texas A&M University, 3255 TAMU, College Station, Texas 77843, United States

[‡]NMR Research Unit, Faculty of Science, University of Oulu, P.O. Box 3000, 90014 Oulu, Finland

[§]Department of Electrical Engineering, Center for Hyperpolarization in Magnetic Resonance, Technical University of Denmark, Building 349, DK-2800 Kgs Lyngby, Denmark

Supporting Information

ABSTRACT: Ultrafast Laplace NMR (UF-LNMR), which is based on the spatial encoding of multidimensional data, enables one to carry out 2D relaxation and diffusion measurements in a single scan. Besides reducing the experiment time to a fraction, it significantly facilitates the use of nuclear spin hyperpolarization to boost experimental sensitivity, because the time-consuming polarization step does not need to be repeated. Here we demonstrate the usability of hyperpolarized UF-LNMR in the context of cell metabolism, by investigating the conversion of pyruvate to lactate in the cultures of mouse 4T1 cancer cells. We show that ^{13}C ultrafast diffusion−T_2 relaxation correlation measurements, with the sensitivity enhanced by several orders of magnitude by dissolution dynamic nuclear polarization (D-DNP), allows the determination of the extra- vs intracellular location of metabolites because of their significantly different values of diffusion coefficients and T_2 relaxation times. Under the current conditions, pyruvate was located predominantly in the extracellular pool, while lactate remained primarily intracellular. Contrary to the small flip angle diffusion methods reported in the literature, the UF-LNMR method does not require several scans with varying gradient strength, and it provides a combined diffusion and T_2 contrast. Furthermore, the ultrafast concept can be extended to various other multidimensional LNMR experiments, which will provide detailed information about the dynamics and exchange processes of cell metabolites.

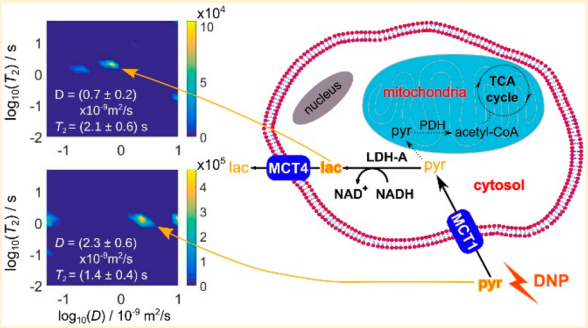

In cancer research, cardiovascular imaging, and diabetes research, metabolic differences between normal and diseased tissues can be accessed noninvasively by nuclear magnetic resonance (NMR).[1,2] Hyperpolarization by dissolution dynamic nuclear polarization (D-DNP) has been shown to provide unprecedented gains in NMR signal.[3] In recent years, D-DNP has enabled the determination of metabolic pathways and measurement of metabolic flux both in cell cultures and in vivo using magnetic resonance imaging (MRI).[4,5] ^{13}C NMR of various hyperpolarized precursors, including pyruvate, glucose, bicarbonate, fumarate, and others, serves as probes for specific metabolic pathways. The observation time window of ^{13}C nuclei is wide because of their long T_1, and their broad chemical shift range facilitates the resolution of metabolites.

A challenge in studies of metabolism by NMR is that compounds inside and outside of cells are not resolved in the spectra. Furthermore, individual cells are smaller than the achieved spatial resolution in MRI. Therefore, only a combination of extracellular and intracellular locations is observed. The separation of these compartments can be achieved through measurement of diffusion.[6] Restrictions in the intracellular environment, such as macromolecular binding and boundaries due to compartmentation, lead to an intracellular diffusion coefficient of metabolites that is significantly smaller than that in the extracellular space. Diffusion magnetic resonance spectroscopy therefore can be used to evaluate membrane transport, which itself can serve as a marker for tumor diagnosis.[7]

However, conventional diffusion measurements,[8,9] which require multiple incremental scans, are a priori not compatible with hyperpolarization, because the signal is short-lived, and repolarization using D-DNP takes place ex situ and with build-up times much longer than the scan time, from tens of minutes to hours. The diffusion contrast becomes available through the use of small flip angle excitations with various diffusion encoding steps. Therefore, ^{13}C hyperpolarized metabolite signals have been distinguished in different cellular compartments in vitro[10] and in vivo.[11]

Received: July 11, 2018
Accepted: August 20, 2018
Published: August 20, 2018

DOI: 10.1021/acs.analchem.8b03096
Anal. Chem. 2018, 90, 11131−11137

Recently, we have shown that multidimensional NMR diffusion and relaxation data[12−14] can be measured with a single scan.[15−19] This method is termed ultrafast Laplace NMR (UF-LNMR). Similar to ultrafast NMR spectroscopy[20−23] as well as single scan one-dimensional diffusion[24−26] and relaxation experiments,[27,28] the method is based on spatial encoding of multidimensional data. The distribution of the relaxation times and/or diffusion coefficients is obtained by a Laplace inversion.[29−31] The single scan approach makes it possible to use hyperpolarized substances to boost the experimental sensitivity by several orders of magnitude.[32,33]

We have previously demonstrated substantial sensitivity enhancements in diffusion−T_2 relaxation ($D-T_2$) correlation UF-LNMR of solvents and hydrocarbons, using hyperpolarization by D-DNP and *para*-hydrogen induced polarization.[16] Here, we extend this technique to the analysis of cell metabolism in biological samples. To enable separation of metabolites by chemical identity, we introduce a chemical shift selective, pulsed-field gradient spin echo (PGSE) based UF $D-T_2$ LNMR experiment, which enabled us to carry out the experiment with a single selective pulse only. This is important, because several selective pulses of extended duration can cause unintended evolution of coherences and significant decay of signal; the pulsed-field gradient stimulated echo (PGSTE) based UF $D-T_2$ experiment used in the previous work[16] would require several selective $\pi/2$ pulses. We show that this experiment enables the differentiation of diffusion coefficients consistent with intracellular and extracellular locations of ^{13}C hyperpolarized pyruvate and its metabolic product lactate in mouse 4T1 breast cancer cells. Contrary to the small flip angle diffusion measurements described above, the UF-LNMR method does not require repetition of experiments with multiple diffusion encoding steps or prior knowledge of diffusion coefficients in the compartments. Furthermore, it provides a combined D and T_2 contrast, which improves the resolution of the components.

EXPERIMENTAL SECTION

Cell Cultures. 4T1 mouse breast cancer cells were maintained as a monolayer and grown in RPMI-1640 medium (ThermoFisher Scientific, Waltham, MA) supplemented with 10% fetal bovine serum and 1% penicillin/streptomycin (10 000 U/mL) in a CO_2 incubator at 37 °C. The cells were passaged serially and used for NMR experiments between passages 3 to 5. Single cell suspensions were derived by trypsinization with 0.1% (w/v) trypsin/0.04% (w/v) ethylenediaminetetraacetic acid (EDTA) in 3 min. For NMR measurements, cells with ∼90% confluency from eight culture plates (surface area = 75 cm^2 per plate; VWR, Radnor, PA) were collected by trypsinization and centrifugation. Cells were resuspended in 0.5 mL of phosphate buffer (0.2 g/L KCl, 0.2 g/L KH_2PO_4, 8.0 g/L NaCl, 1.15 g/L Na_2HPO_4, pH 7.25). The cell suspension was transferred to the first injection loop, for nonhyperpolarized sample, of a liquid driven sample injector for D-DNP NMR spectroscopy.[34] This transfer occurred shortly before the NMR experiment, in order to maintain cell viability. The number of cells was ∼2.5 × 10^8 in the injection loop, and ∼1 × 10^8 after injection into a flow cell preinstalled in the NMR magnet.

Hyperpolarization. A solution of 1 M $^{13}C_1$-pyruvate (Cambridge Isotopes, Tewksbury, MA) with 15 mM Tris[8-carboxy-2,2,6,6-tetrakis(2-hydroxyethyl)benzo[1,2-*d*:4,5-*d*′]-bis[1,3]-dithiol-4-yl]methyl free radical sodium salt (OX063; Oxford Instruments, Abingdon, U.K.) was prepared in a D_2O/ethylene glycol (2/3 v/v) glass forming mixture. This sample solution (8 μL) was hyperpolarized on ^{13}C for 3 h at 1.4 K in a HyperSense DNP polarizer (Oxford Instruments), by irradiating microwaves with 60 mW power at a frequency of 93.974 GHz in a 3.35 T magnetic field. The hyperpolarized sample was rapidly dissolved in preheated phosphate buffer (10 mM Na_2HPO_4, 100 mg/L EDTA, pH 7.4) and transferred into the second loop of the liquid driven sample injector. The cell and hyperpolarized pyruvate samples were subsequently driven into a mixer and then into a flow cell preinstalled in the magnet, using water from a high pressure syringe pump (model 1000D, Teledyne ISCO, Lincoln, NE). The final temperature was 308 K during NMR measurement. This temperature was determined by measuring a ^{1}H hyperpolarized spectrum of ethylene glycol (EG) sample (EG/D_2O (3/2, v/v) and 15 mM 4-hydroxy-2,2,6,6-tetramethylpiperidine-1-oxyl (TEMPOL) free radical (Sigma-Aldrich, St. Louis, MO)) as a chemical shift thermometer[35] with the same injection time as used in the experiments. The liquid state spin polarization of $^{13}C_1$-pyruvate was ∼20%.

NMR Spectra. Spectra were acquired on a 400 MHz NMR spectrometer with a triple resonance TXI probe (Bruker Biospin, Billerica, MA) and installed NMR flow cell. The time evolution of ^{13}C signals was determined using the pulse sequence (trigger−[G_z−α−acquire]$_{xn}$). A total of n = 64 transients were acquired over a duration of 320 s. A pulsed-field gradient G_z(45.5 G/cm, 1 ms) was applied for attenuation of coherences present from the previous scans. The small flip angle α of the excitation pulse was 10°, with pulse strength $(\gamma B_1)/2\pi$ = 17.86 kHz. In each scan, a total of 12 000 complex points were acquired with an acquisition time of 0.5 s. The NMR experiment was triggered after 800 ms of injection and mixing time and 5 s of waiting time.

UF $D-T_2$. UF $D-T_2$ LNMR measurements incorporating chemical shift selection on pyruvate or lactate ^{13}C resonances at 170.4 or 182.6 ppm were performed in single scans. The experiments were carried out for 20 s after the injection. In the pulse sequence, a PGSE based chemical shift selective excitation pulse was used for the UF $D-T_2$ LNMR measurements, where ^{13}C resonances of pyruvate or lactate were selectively excited. As shown in Figure 1, the first $\pi/2$ was a selective 90° Gaussian pulse with 1% truncation level, applied at the center of a ^{13}C resonance. The pulse duration was 8488 μs and excitation bandwidth was 249 Hz. The following two π pulses were frequency-swept chirp pulses with 10% smoothing on the edges. The pulse duration (t_{chirp}) was 2.5 ms, bandwidth was 48.7 kHz, and $(\gamma B_{1max})/2\pi$ was 3.94 kHz. The power of

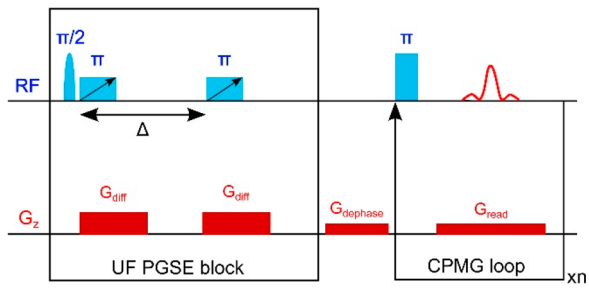

Figure 1. Ultrafast $D-T_2$ correlation experiment used in the present work.

DOI: 10.1021/acs.analchem.8b03096
Anal. Chem. 2018, 90, 11131−11137

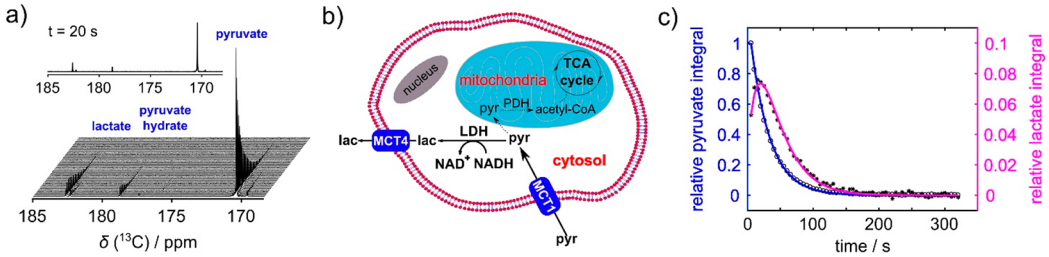

Figure 2. (a) Stacked plot of ^{13}C spectra measured with a time interval of 5 s after injection of hyperpolarized $^{13}C_1$-pyruvate to 4T1 cancer cells. The inset shows the spectrum at the time point of 20 s, where the $D-T_2$ measurements were performed. (b) Scheme of a cancer cell, indicating membrane transport of pyruvate and lactate as well as the associated metabolic pathways.[43] MCT; monocarboxylate transporters, LDH; lactate dehydrogenase, PDH; pyruvate dehydrogenase. (c) Integrals and kinetic fit of pyruvate and lactate signals as a function of time. All signal integrals were normalized with the maximum pyruvate signal integral.

the π pulse in the CPMG loop was $(\gamma B_1)/2\pi$ = 17.86 kHz. Pulsed-field gradients were trapezoidal shaped with ramp time of 1 ms. Gradients were applied with amplitudes G_{diff} = 36.4 G/cm, $G_{dephase}$ = 2.3 G/cm, G_{read} = 2.3 G/cm, and durations $t_{G,diff}$ = 5.0 ms, $t_{G,dephase}$ = 8.9 ms, $t_{G,read}$ = 16.9 ms. The diffusion delay was Δ = 50 ms. The simultaneously applied G_{diff} and frequency-swept π pulse resulted in a spatial dependence of the effective length of G_{diff} that a spin experiences in the range of δ_{eff} = 0···5 ms. The number of complex points in each echo was 256, and altogether, 64 echoes were collected in the CPMG loop with the time interval of 20 ms. The spectral width was 25 kHz. The total experiment time was t_{exp} = 1.4 s.

Reference Diffusion Experiments. A conventional pulsed-field gradient stimulated echo experiment (PGSTE) was used for diffusion measurements without hyperpolarization, using thermally polarized ^1H signals of a pyruvate sample previously used in the hyperpolarized $D-T_2$ measurement without cell suspension (Figure S-1). This pulse sequence consisted of $[p1 - G1-p1 - \tau_1/G2-p1-G3-acquire]_{\times n}$. 90° hard pulses p1 were applied with $(\gamma B_1)/2\pi$ = 28.97 kHz. Diffusion encoding and decoding gradients, G1 and G3, respectively, were simultaneously and linearly increased from 1.17 to 55.58 G/cm with n = 16 steps. The diffusion time Δ, which is from the start of G1 to the start of G3, was 80 ms. The gradient duration δ was 0.9 ms. The delay τ_1 = 78 ms. A homospoil gradient G2 was applied with amplitude −10.02 G/cm and duration $\delta_{homospoil}$ = 0.85 ms. The z-gradient strength was calibrated using a H_2O sample with known diffusion coefficient of $2.3 \cdot 10^{-9}$ m^2/s at T = 298.2 K (Figure S-2, details of calibration below).

A conventional PGSTE experiment was used for calibration of z-gradient strength G. ^1H signals of thermally polarized water were measured at T = 298.2 K. The pulse sequence is the same as that used for diffusion measurement of a thermally polarized pyruvate sample (Figure S-1). Experimental parameters are $(\gamma B_1)/2\pi$ = 28.57 kHz, Δ = 100 ms, δ = 1.1 ms, τ_1 = 98 ms, and $\delta_{homospoil}$ = 0.8 ms.

Residual motions in the sample after injection were assessed using the same single scan ultrafast $D-T_2$ measurement as in the cell metabolism experiments. A selective 90° Gaussian pulse is applied at the center of ^1H resonances of water at 4.7 ppm (see Table S-1 for experimental parameters). As shown in Figure S-3, the sample was already stationary after 20 s of stabilization, with an apparent diffusion coefficient of $(3.3 \pm 1.0) \cdot 10^{-9}$ m^2/s, compared to the reference value of $2.9 \cdot 10^{-9}$ m^2/s.[36] The agreement of these diffusion coefficients within error limits indicates that the D-DNP sample is nearly stationary during data acquisition, validating the stopped-flow injection into the NMR flow cell. In this approach, the flow path is pinched both in the inlet and outlet tubing after delivering the sample into the cell, therefore preventing large scale flow of the sample during NMR measurement.[34] Furthermore, no gas bubbles were observed at the time of measurement, which was also confirmed by a one-dimensional imaging experiment (Figure S-4).

A pulsed-field gradient echo experiment was used for a one-dimensional image measurement. The pulse sequence consists of elements [p1−G1−τ_1−p2−G2/acquire]. p1 and p2 are 90° and 180° hard pulses with $\gamma B_1/(2\pi)$ = 27.03 kHz. G1 and G2 are denoted as defocusing and refocusing pulsed-field gradients with gradient strength 1.95 G/cm. The gradient duration of G2 = 17.88 ms is twice as long as that of G1. The delay τ_1 = 1.1 ms. The coincidence of red and black curves in Figure S-4 demonstrates that no gas bubbles were observed after 15 s waiting time.

Data Analysis. For determining time evolution from ^{13}C NMR spectra, the raw data was filled to 65 536 complex data points and multiplied with an exponential window function with a line broadening of 0.3 Hz before Fourier transform, using TOPSPIN 3.5 (Bruker Biospin). All peak integration and curve fitting were conducted using the Matlab program (MathWorks, Natick, MA).

For a hyperpolarized ^{13}C UF $D-T_2$ experiment, the data was first Fourier transformed along the direction of spatial encoding. 33 data points were in the encoding region. Then, the data outside, close to the beginning, and at the end of the encoding region was removed, see Refs 16,37. After this, the number of data points in the diffusion and T_2 dimensions were 19 and 64, respectively. The range of the effective diffusion gradient pulse length was δ_{eff} = [0.94 ms, 3.75 ms], and the time range was t_{CPMG} = [0.02 ms, 1.28 ms]. The 2D diffusion coefficient and T_2 relaxation time distributions were determined using a Laplace inversion program provided by P. Callaghan (Victoria University of Wellington, New Zealand)[38] and based on a previously published method.[29] The size of the $D-T_2$ data was 25 × 19. The distributions covered the following ranges: T_2 = [0.01 s, 50 s] and D = [5 × 10^{-11} m^2/s, 10^{-8} m^2/s].

For the ^1H UF $D-T_2$ experiment as shown in Figure S-3, a Laplace inversion was applied as described above. A range of δ_{eff} = [0.87 ms, 2.63 ms] and t_{CPMG} = [0.02 ms, 1.28 ms] was used. 63 data points were in the encoding region. The number of data points in the diffusion and T_2 dimensions were 29 and 64, respectively. The $D-T_2$ data size was 20 × 40. Correlation

DOI: 10.1021/acs.analchem.8b03096
Anal. Chem. 2018, 90, 11131−11137

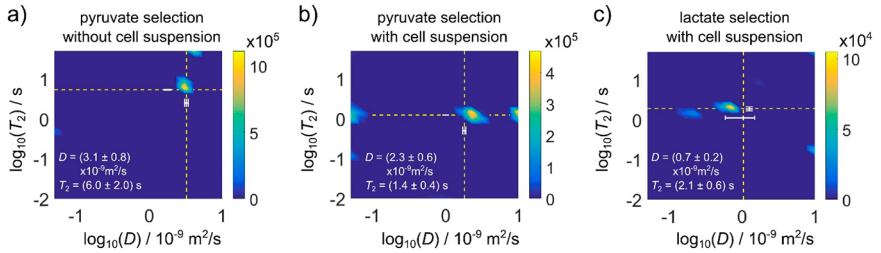

Figure 3. Chemically selective ultrafast $D-T_2$ map of (a) pyruvate without cell suspension, (b) pyruvate in cell suspension, and (c) lactate in cell suspension. The D and T_2 values shown in the figures correspond to the maxima of the peaks. The uncertainties are estimated from the width of the peaks. The dashed lines and white error bars are results from the single exponential fits of the data along the D or T_2 directions (see Figures S-7 and S-8 in Supporting Information).

diagrams covered ranges $T_2 = [0.01\ \text{s}, 20\ \text{s}]$ and $D = [5 \times 10^{-11}\ \text{m}^2/\text{s}, 10^{-8}\ \text{m}^2/\text{s}]$.

Modeling of Signal Intensities in the Spectra. Signal intensities in the hyperpolarized ^{13}C spectra (see Figure 2), $M_{z,\text{pyr}}$ and $M_{z,\text{lac}}$, can be quantitatively modeled using the following equations[39]

$$\frac{dM_{z,\text{pyr}}(t)}{dt} = -k_{\text{pyr-lac}} \times M_{z,\text{pyr}}(t) - (R_{1,\text{pyr}} + \lambda) \times M_{z,\text{pyr}}(t) \quad (1)$$

$$\frac{dM_{z,\text{lac}}(t)}{dt} = k_{\text{pyr-lac}} \times M_{z,\text{pyr}}(t) - (R_{1,\text{lac}} + \lambda) \times M_{z,\text{lac}}(t) \quad (2)$$

The observed rate constant for the conversion from pyruvate to lactate, $k_{\text{pyr-lac}}$, depends on the cell density in the experiment. It includes contributions from the lactate dehydrogenase activity as well as from the membrane transport of pyruvate. Since no statistical improvement in the fit was found by considering the conversion of lactate to pyruvate, the rate constant $k_{\text{lac-pyr}}$ is neglected. $R_{1,\text{pyr}}$ and $R_{1,\text{lac}}$ are the relaxation rates on the carbonyl sites. The parameter $\lambda = -\ln(\cos(\alpha))/\Delta t$, with $\alpha = 10°$ and $\Delta t = 5$ s as the time interval between two scans, accounts for signal depletion due to the small flip angle pulses. For the experimental data from Figure 2c, the resulting fit parameters are $k_{\text{pyr-lac}} = 6.5 \cdot 10^{-3}\ \text{s}^{-1}$, $T_{1,\text{pyr}} = 41$ s, and $T_{1,\text{lac}} = 19$ s.

RESULTS AND DISCUSSION

Turnover of Hyperpolarized Pyruvate. The time evolution of a series of 1D ^{13}C spectra of hyperpolarized $^{13}C_1$-pyruvate with 4T1 cancer cells injected into the NMR flow cell is shown in Figure 2a (see Experimental Section). The ^{13}C signal of pyruvate appears at 170.4 ppm, and the metabolic product lactate is visible at 182.6 ppm. A further signal at 178.7 ppm corresponds to pyruvate hydrate, which is formed by a nonbiological process. The observation of a strong lactate signal is expected for cancer cells, where the glycolytic pathway is strongly favored even in the presence of sufficient oxygen (Figure 2b).[40] As a result of the combined effects of reaction kinetics, T_1 relaxation, and radio frequency pulses,[41] the pyruvate signal shows a monoexponential decay, which is paralleled by an initial increase of lactate signal. The integrated lactate signal reaches its maximum after 20 s (Figure 2c). At that point, it is approximately 12.5 times lower than the initial signal of pyruvate. A lower signal of the metabolic product is also expected because of the interplay of the different rate constants affecting the signal. On the basis of the quantitative modeling of the signal intensities (see Experimental Section), we determined that the rate constant of the conversion from pyruvate to lactate is $k_{\text{pyr-lac}} = 6.5 \cdot 10^{-3}\ \text{s}^{-1}$ under the given experimental conditions with $\sim 1 \times 10^8$ 4T1 cancer cells, and the T_1 relaxation times of pyruvate and lactate are $T_{1,\text{pyr}} = 41$ s and $T_{1,\text{lac}} = 19$ s. The T_1 values match the values reported for an in vitro experiment using T47D human breast cancer cells ($T_{1,\text{pyr}} \approx 45$ s and $T_{1,\text{lac}} \approx 19$ s) performed under comparable experimental conditions.[42]

Ultrafast $D-T_2$ Maps. The modified pulse sequence of the UF $D-T_2$ experiment used in the present work, shown in Figure 1, begins with a chemical shift selective $\pi/2$ pulse used for the excitation of either the pyruvate or lactate signal. The spatial encoding of diffusion data is based on an ultrafast pulsed-field gradient spin echo (UF-PGSE) sequence, employing the spin−echoes created by two successive adiabatic frequency-swept chirp π pulses.[37] UF-PGSE part is followed by the CPMG loop for T_2 relaxation, during which the magnetization profile is read by using the principles of MRI.[16] The experiment results in $D-T_2$ data equivalent to a traditional measurement in a single scan, with the experiment time of only 1.4 s (see Experimental Section).

Hyperpolarized UF $D-T_2$ experiments were carried out for pyruvate without cell suspension as well as pyruvate and lactate in the 4T1 cell suspension by selectively exciting one of the metabolite signals for 20 s after the sample injection. $D-T_2$ maps resulting from 2D Laplace inversion of the measured data are shown in Figure 3. Hyperpolarized pyruvate without cell suspension results in a single signal with $T_2 = (6.0 \pm 2.0)$ s and $D = (3.1 \pm 0.8) \cdot 10^{-9}\ \text{m}^2/\text{s}$ (Figure 3a). This diffusion coefficient is consistent with that obtained using a conventional PGSTE pulse sequence on a stationary, nonhyperpolarized sample at $T = 308$ K, which yielded $D = (2.2 \pm 0.4) \cdot 10^{-9}\ \text{m}^2/\text{s}$ (see Experimental Section). The T_2 is shortened compared to values that would be obtained with a basic spin−echo pulse sequence because of the use of magnetic field gradients for reading the magnetization profile.[15,16]

In the presence of cell suspension, the signal obtained with selective excitation of the pyruvate-$^{13}C_1$ resonance yields a D value of $(2.3 \pm 0.6) \cdot 10^{-9}\ \text{m}^2/\text{s}$ (Figure 3b). A $D-T_2$ map acquired in a separate experiment with selective excitation of the lactate resonance is shown in Figure 3c. The diffusion coefficient of lactate was determined as $(0.7 \pm 0.2) \cdot 10^{-9}\ \text{m}^2/\text{s}$. Two additional repetitions (Figure S-5), which were performed to assess reproducibility, resulted in $(0.7 \pm 0.3) \cdot 10^{-9}\ \text{m}^2/\text{s}$ and $(1.0 \pm 0.3) \cdot 10^{-9}\ \text{m}^2/\text{s}$. The obtained diffusion coefficient is three times lower than that of pyruvate. Since pyruvate and lactate show similar diffusion coefficients in aqueous solution alone[44] ($D_{\text{pyr}} = (1.12 \pm 0.04) \cdot 10^{-9}\ \text{m}^2/\text{s}$ and $D_{\text{lac}} = (1.00 \pm 0.01) \cdot 10^{-9}\ \text{m}^2/\text{s}$ measured in 50 mM phosphate

DOI: 10.1021/acs.analchem.8b03096
Anal. Chem. 2018, 90, 11131−11137

buffer solution at 27 °C in a 14.1 T magnetic field), the observed difference suggests that, here, the two signals stem from different environments. Pyruvate is converted into lactate in the cytoplasm, and therefore, the lower diffusion coefficient of lactate is explained by restricted diffusion inside the cells due to increased viscosity, compartmentalization, and interactions with macromolecules. At the same time, this data indicates that lactate that has exported from cells at the time of measurement does not significantly contribute to the observed signal. Conversely, the primary pyruvate pool in this experiment appears to be extracellular.

Diffusion coefficients of lactate and pyruvate, D_{lac} and D_{pyr}, shown in Figure 3b,c, are consistent with $D_{lac} = (0.8 \pm 0.2) \cdot 10^{-9}$ m^2/s and $D_{pyr} = (1.7 \pm 0.6) \cdot 10^{-9}$ m^2/s values measured using a surface coil in an EL-4 murine lymphoma tumor in vivo at 37 °C by Kettunen et al.[45] They are also consistent with $D_{pyr} = (1.94 \pm 0.07) \cdot 10^{-9}$ m^2/s and $D_{lac} = (1.06 \pm 0.15) \cdot 10^{-9}$ m^2/s measured in MCF-7 tumor cell spheroids in vitro at 37 °C by Schilling et al.[10] In these reference values, the observed D_{pyr} is presumed to predominantly stem from an extracellular pool of pyruvate and the observed D_{lac} predominantly stems from an intracellular pool of lactate. Therefore, the comparison confirms the reliability of the UF LNMR method.

In addition to D, the observed T_2 values are different in each case shown in Figure 3. While the reduced T_2 in (b) would be expected because of the higher viscosity of the sample compared to (a), which leads to longer rotational correlation time, an increase in T_2 in (c) compared to (b) cannot be explained in this way. Another effect that needs to be taken into consideration is a coupling between diffusion and T_2 relaxation measurement. A magnetic field gradient at the time of signal acquisition increases the echo attenuation due to molecular self-diffusion,[46] leading to a shortened observed T_2 value. A calculation of this effect for the conditions observed in the lactate and pyruvate signals is shown in Figure S-6. Irrespective of the origin of the observed changes in T_2, this parameter takes a different value for each of the species observed in Figure 3, thereby improving the contrast between the species.

The current ultrafast experiment employs a 90° selective pulse to excite a metabolite peak of interest. Such selection may be advantageous for spectra with multiple peaks, simplifying the identification of peaks. We recorded also a data set without selective excitation. Although both pyruvate and lactate signals were simultaneously excited in this experiment, a resulting $D-T_2$ map did not show multiple resolved signals. The ratio of pyruvate to lactate signal intensity is ∼10, with the SNR of $^{13}C_1$-pyruvate ≈ 170. Such a SNR may not be sufficient to resolve these two components with significantly different intensities in $D-T_2$ maps, as shown in a previous simulation.[16] However, they can be resolved through chemical shift selective excitation as demonstrated here. Since the contribution of extracellular lactate signal and intracellular pyruvate signal is small, these species were not observed in the $D-T_2$ maps. In consequence, a single intracellular lactate signal and a single extracellular pyruvate signal was observed in each $D-T_2$ map. Analysis of single D and T_2 traces with single exponential fits, shown in Figure S-7, are further possible, because only a single signal component is observed. This analysis results in D and T_2 values, which are in good agreement with the values obtained from the Laplace inversions (see Figure 3). In cases where the contribution of lactate signal and pyruvate signal from the extra- and intracellular spaces is sufficient, two resolved intra- and extracellular lactate (pyruvate) signals are expected on a $D-T_2$ map obtained with selective excitation of the lactate (pyruvate) resonance in the presence of cell suspension.

One benefit of using Laplace inversion to determine diffusion is that no prior knowledge of the value of the diffusion coefficient or the number of components that are present is needed. To determine the D value, the analysis initializes with a range of D values, for instance [10^{-12}, 10^{-7} m^2/s], which corresponds to D of most molecules. After the initial analysis, the parameter range can be narrowed. In addition, with sufficient signal-to-noise ratio, the heterogeneity of a spin system can be resolved by showing signals of diffusion coefficients and T_2 relaxation for different components at different positions on a $D-T_2$ map. In contrast, typical analysis methods for signals showing multiexponential decay, as they are encountered in diffusion NMR, first require the choice of an adequate fitting model based on the known or assumed number of components present.[6,47−49]

In the UF LNMR $D-T_2$ experiment, spatial encoding results in the acquisition of an entire data set in a single scan. Therefore, the acquisition time can be reduced by several orders of magnitude compared to a conventional measurement. Here, sensitivity is enhanced by the use of hyperpolarization. This makes it possible to measure diffusion and T_2 relaxation based on ^{13}C signals of pyruvate and lactate with concentrations as low as ∼10 and ∼1 mM, and within 1.4 s. The detection of ^{13}C signal may have more specificity than the ^1H signals that would be acquired without hyperpolarization, in particular, in complex samples containing many metabolites.

The identification of intracellular metabolites is of importance for the interpretation of rate constants obtained from in vitro metabolic studies using D-DNP hyperpolarization. Specifically, a potential application of this method is the assessment of membrane permeability. Necrosis of cancer cells due to the use of anticancer drugs can cause the cell membrane to lose its selectivity. Molecules, which are normally transported across the cell membrane by transmembrane proteins, are free to diffuse in or out of the cells more rapidly. Schilling et al.[10] has reported a decreased ratio of D_{pyr} over D_{lac}, as the fraction of dead cells increases during progressive membrane permeabilization. This ratio can serve as a marker for monitoring the pathological changes and treatment response in cancer. Second, it has been found that upregulation of MCT is associated with malignancy of cancer cells.[50] By measuring the change of intra- and extracellular proportion of metabolites, such as lactate, as a function of time after the injection of hyperpolarized precursor, such as pyruvate, transport rates can be derived, which opens the way to assess the activity of MCTs.[51]

Similar pulse sequences may in the future also be applicable in an in vivo context, such as for the characterization of tumors. Spatial encoding would in this case be realized over a homogeneous image region, determined by a pilot image prior to the acquisition of the diffusion data. The localization of lactate specifically may assist in the determination of tumor aggressiveness, which is linked to lactate export.[52]

CONCLUSIONS

In summary, we have described ultrafast $D-T_2$ correlation LNMR as a tool to distinguish intra- vs extracellular metabolites in the study of cellular metabolism. This experiment simultaneously provides contrast in the diffusion

DOI: 10.1021/acs.analchem.8b03096
Anal. Chem. 2018, 90, 11131−11137

and T_2 relaxation parameters, therefore enhancing the ability to localize a metabolite. The correlation map can be acquired in a single scan, resulting in a shorter experiment time than for other diffusion measurements. The single scan nature also renders the method inherently compatible with the use of nonrenewable hyperpolarization to provide a large sensitivity enhancement. Using ^{13}C hyperpolarization, we demonstrated the identification of pools of lactate and pyruvate with significantly different self-diffusion coefficients in cultures of mouse 4T1 breast cancer cells by this method. The observed differences are consistent with an expected difference in diffusion coefficients in the case of predominantly intracellular and extracellular location of the two metabolites. For determining diffusion by Laplace inversion, no prior knowledge of the value of the diffusion coefficient or the number of components that are present is required. Beyond the measurement of diffusion, the basic scheme of hyperpolarized UF LNMR can further be adapted to investigate other parameters for characterizing dynamic and exchange processes.

■ ASSOCIATED CONTENT

Supporting Information

The Supporting Information is available free of charge on the ACS Publications website at DOI: 10.1021/acs.analchem.8b03096.

Figures showing determination of self-diffusion coefficient of pyruvate, *z*-gradient strength calibration, measurement and comparison of $D-T_2$ maps and coil image profiles of stationary water and water injected into the flow cell, additional data with selection of lactate signal in cell suspension, calculation of T_2 relaxation parameters, analysis of single D and T_2 traces, and diffusion coefficient fitting of 64 echos of hyperpolarized $D-T_2$ data are shown; one table listing experimental parameters for $D-T_2$ measurement of thermally polarized water (PDF)

■ AUTHOR INFORMATION

Corresponding Authors

*E-mail: chilty@tamu.edu (C.H.)

*E-mail: ville-veikko.telkki@oulu.fi (V.V.T.)

ORCID

Ville-Veikko Telkki: 0000-0003-0846-6852

Christian Hilty: 0000-0003-2539-2568

Present Address

[‖]Guannan Zhang, Department of Chemistry, Duke University, Durham, North Carolina 27708, United States

Notes

The authors declare no competing financial interest.

■ ACKNOWLEDGMENTS

We acknowledge the generous support provided by the European Research Council (ERC) under Horizon 2020 (H2020/2018-2022/ERC grant agreement no. 772110), the Academy of Finland (grant numbers 289649 and 294027), the National Science Foundation (Grant CHE-1362691), the Ji and Li Family Foundation, and the Welch Foundation (Grant A-1658). We thank Dr. Wenshe Liu and Wei Wang (Texas A&M University) for use of and assistance with the cell culturing facility.

■ REFERENCES

(1) Amoêdo, N. D.; Valencia, J. P.; Rodrigues, M. F.; Galina, A.; Rumjanek, F. D. *Biosci. Rep.* **2013**, *33* (6), 865−873.

(2) DeBerardinis, R. J.; Thompson, C. B. *Cell* **2012**, *148* (6), 1132−1144.

(3) Ardenkjær-Larsen, J. H.; Fridlund, B.; Gram, A.; Hansson, G.; Hansson, L.; Lerche, M. H.; Servin, R.; Thaning, M.; Golman, K. *Proc. Natl. Acad. Sci. U. S. A.* **2003**, *100* (18), 10158−10163.

(4) Serrao, E. M.; Brindle, K. M. *Front. Oncol.* **2016**, *6*, 59.

(5) Siddiqui, S.; Kadlecek, S.; Pourfathi, M.; Xin, Y.; Mannherz, W.; Hamedani, H.; Drachman, N.; Ruppert, K.; Clapp, J.; Rizi, R. *Adv. Drug Delivery Rev.* **2017**, *113*, 3.

(6) Koelsch, B. L.; Sriram, R.; Keshari, K. R.; Leon Swisher, C.; Van Criekinge, M.; Sukumar, S.; Vigneron, D. B.; Wang, Z. J.; Larson, P. E. Z.; Kurhanewicz, J. *J. Magn. Reson.* **2016**, *270*, 115−123.

(7) Tsuruda, J. S.; Chew, W. M.; Moseley, M. E.; Norman, D. *Magn. Reson. Med.* **1991**, *19* (2), 316−320.

(8) Stejskal, E. O.; Tanner, J. E. *J. Chem. Phys.* **1965**, *42* (1), 288−292.

(9) Tanner, J. E. *J. Chem. Phys.* **1970**, *52* (5), 2523−2526.

(10) Schilling, F.; Düwel, S.; Köllisch, U.; Durst, M.; Schulte, R. F.; Glaser, S. J.; Haase, A.; Otto, A. M.; Menzel, M. I. *NMR Biomed.* **2013**, *26* (5), 557−568.

(11) Koelsch, B. L.; Reed, G. D.; Keshari, K. R.; Chaumeil, M. M.; Bok, R.; Ronen, S. M.; Vigneron, D. B.; Kurhanewicz, J.; Larson, P. E. Z. *Magn. Reson. Med.* **2015**, *74* (3), 622−633.

(12) Callaghan, P. T. *Translational Dynamics and Magnetic Resonance: Principles of Pulsed Gradient Spin Echo NMR*; Oxford University Press, 2011.

(13) Song, Y.-Q. *J. Magn. Reson.* **2013**, *229*, 12−24.

(14) Bernin, D.; Topgaard, D. *Curr. Opin. Colloid Interface Sci.* **2013**, *18* (3), 166−172.

(15) Ahola, S.; Telkki, V.-V. *ChemPhysChem* **2014**, *15* (8), 1687−1692.

(16) Ahola, S.; Zhivonitko, V. V.; Mankinen, O.; Zhang, G.; Kantola, A. M.; Chen, H.-Y.; Hilty, C.; Koptyug, I. V.; Telkki, V.-V. *Nat. Commun.* **2015**, *6*, 8363.

(17) King, J. N.; Lee, V. J.; Ahola, S.; Telkki, V.-V.; Meldrum, T. *Angew. Chem., Int. Ed.* **2016**, *55* (16), 5040−5043.

(18) King, J. N.; Fallorina, A.; Yu, J.; Zhang, G.; Telkki, V.-V.; Hilty, C.; Meldrum, T. *Chem. Sci.* **2018**, *9* (28), 6143−6149.

(19) Mankinen, O.; Hollenbach, J.; Ahola, S.; Matysik, J.; Telkki, V.-V. *Microporous Mesoporous Mater.* **2018**, *269*, 75−78.

(20) Frydman, L.; Scherf, T.; Lupulescu, A. *Proc. Natl. Acad. Sci. U. S. A.* **2002**, *99* (25), 15858−15862.

(21) Pelupessy, P. *J. Am. Chem. Soc.* **2003**, *125* (40), 12345−12350.

(22) Tal, A.; Frydman, L. *Prog. Nucl. Magn. Reson. Spectrosc.* **2010**, *57* (3), 241−292.

(23) Akoka, S.; Giraudeau, P. *Magn. Reson. Chem.* **2015**, *53* (11), 986−994.

(24) Thrippleton, M. J.; Loening, N. M.; Keeler, J. *Magn. Reson. Chem.* **2003**, *41* (6), 441−447.

(25) Shrot, Y.; Frydman, L. *J. Magn. Reson.* **2008**, *195* (2), 226−231.

(26) Guduff, L.; Kuprov, I.; van Heijenoort, C.; Dumez, J.-N. *Chem. Commun.* **2017**, *53* (4), 701−704.

(27) Loening, N. M.; Thrippleton, M. J.; Keeler, J.; Griffin, R. G. *J. Magn. Reson.* **2003**, *164* (2), 321−328.

(28) Smith, P. E. S.; Donovan, K. J.; Szekely, O.; Baias, M.; Frydman, L. *ChemPhysChem* **2013**, *14* (13), 3138−3145.

(29) Venkataramanan, L.; Song, Y.-Q.; Hurlimann, M. D. *IEEE Trans. Signal Process.* **2002**, *50* (5), 1017−1026.

(30) Song, Y.-Q.; Venkataramanan, L.; Hürlimann, M. D.; Flaum, M.; Frulla, P.; Straley, C. *J. Magn. Reson.* **2002**, *154* (2), 261−268.

(31) Granwehr, J.; Roberts, P. J. *J. Chem. Theory Comput.* **2012**, *8* (10), 3473−3482.

(32) Frydman, L.; Blazina, D. *Nat. Phys.* **2007**, *3* (6), 415−419.

(33) Mishkovsky, M.; Frydman, L. *ChemPhysChem* **2008**, *9* (16), 2340−2348.

DOI: 10.1021/acs.analchem.8b03096
Anal. Chem. 2018, 90, 11131−11137

(34) Chen, H.-Y.; Hilty, C. *ChemPhysChem* **2015**, *16* (12), 2646−2652.
(35) Ammann, C.; Meier, P.; Merbach, A. *J. Magn. Reson. (1969-1992)* **1982**, *46* (2), 319−321.
(36) Holz, M.; Heil, S. R.; Sacco, A. *Phys. Chem. Chem. Phys.* **2000**, *2* (20), 4740−4742.
(37) Ahola, S.; Mankinen, O.; Telkki, V.-V. *Magn. Reson. Chem.* **2017**, *55* (4), 341−347.
(38) Godefroy, S.; Callaghan, P. T. *Magn. Reson. Imaging* **2003**, *21* (3−4), 381−383.
(39) McConnell, H. M. *J. Chem. Phys.* **1958**, *28* (3), 430−431.
(40) Warburg, O. *Science* **1956**, *123* (3191), 309−314.
(41) Zeng, H.; Lee, Y.; Hilty, C. *Anal. Chem.* **2010**, *82* (21), 8897−8902.
(42) Harris, T.; Eliyahu, G.; Frydman, L.; Degani, H. *Proc. Natl. Acad. Sci. U. S. A.* **2009**, *106* (43), 18131−18136.
(43) Feron, O. *Radiother. Oncol.* **2009**, *92* (3), 329−333.
(44) Koelsch, B. L.; Keshari, K. R.; Peeters, T. H.; Larson, P. E. Z.; Wilson, D. M.; Kurhanewicz, J. *Analyst* **2013**, *138* (4), 1011.
(45) Kettunen, M. I.; Kennedy, B. W. C.; Hu, D.; Brindle, K. M. *Magn. Reson. Med.* **2013**, *70* (5), 1200−1209.
(46) Stepišnik, J.; Lasič, S.; Mohorič, A.; Serša, I.; Sepe, A. *J. Magn. Reson.* **2006**, *182* (2), 195−199.
(47) Van Zijl, P. C.; Moonen, C. T.; Faustino, P.; Pekar, J.; Kaplan, O.; Cohen, J. S. *Proc. Natl. Acad. Sci. U. S. A.* **1991**, *88* (8), 3228−3232.
(48) Inglis, B. A.; Bossart, E. L.; Buckley, D. L.; Wirth, E. D.; Mareci, T. H. *Magn. Reson. Med.* **2001**, *45* (4), 580−587.
(49) Tanner, J. E.; Stejskal, E. O. *J. Chem. Phys.* **1968**, *49* (4), 1768−1777.
(50) Ullah, M. S.; Davies, A. J.; Halestrap, A. P. *J. Biol. Chem.* **2006**, *281* (14), 9030−9037.
(51) Reineri, F.; Daniele, V.; Cavallari, E.; Aime, S. *NMR Biomed.* **2016**, *29* (8), 1022−1027.
(52) San-Millán, I.; Brooks, G. A. *Carcinogenesis* **2017**, *38* (2), 119−133.

DOI: 10.1021/acs.analchem.8b03096
Anal. Chem. 2018, 90, 11131−11137